

# A Green-Absorbing, Red-Fluorescent Phenalenone-Based Photosensitizer as a Theranostic Agent for Photodynamic Therapy

Esther G. Kaye, Karishma Kailass, Oleg Sadovski, and Andrew A. Beharry\*

Cite This: <https://doi.org/10.1021/acsmchemlett.1c00284>

Read Online

ACCESS |

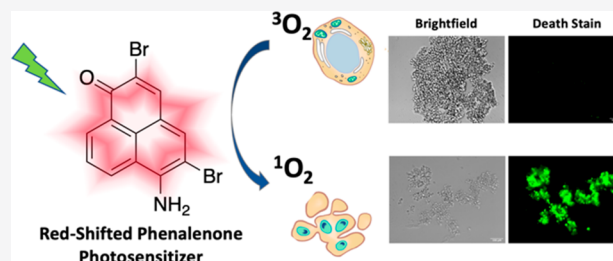
Metrics &amp; More

Article Recommendations

Supporting Information

**ABSTRACT:** Phenalenone is a synthetically accessible, highly efficient photosensitizer with a near-unity singlet oxygen quantum yield. Unfortunately, its UV absorption and lack of fluorescence has made it unsuitable for fluorescence-guided photodynamic therapy against cancer. In this work, we synthesized a series of phenalenone derivatives containing electron-donating groups to red-shift the absorption spectrum and bromine(s) to permit good singlet oxygen production via the heavy-atom effect. Of the derivatives synthesized, the phenalenone containing an amine at the 6-position with bromines at the 2- and 5-positions (OE19) exhibited the longest absorption wavelength (i.e., green) and produced both singlet oxygen and red fluorescence efficiently. OE19 induced photocytotoxicity with nanomolar potency in 2D cultured PANC-1 cancer cells as well as light-induced destruction of PANC-1 spheroids with minimal dark toxicity. Overall, OE19 opens up the possibility of employing phenalenone-based photosensitizers as theranostic agents for photodynamic cancer therapy.

**KEYWORDS:** Photodynamic therapy, photosensitizer, fluorescence, phenalenone, theranostic



Photodynamic therapy (PDT) is a cancer treatment known for its minimal invasiveness and noncumulative resistance compared with traditional therapies.<sup>1</sup> The procedure uses three components: a photosensitizer (PS), light, and molecular oxygen. Once the PS absorbs an appropriate wavelength of light, it undergoes intersystem crossing to the triplet excited state (<sup>3</sup>T), from which its energy is transferred either to molecular oxygen (<sup>3</sup>O<sub>2</sub>) to generate singlet oxygen (<sup>1</sup>O<sub>2</sub>) (Type II mechanism) or to biomolecules to produce radical species (Type I mechanism),<sup>2</sup> with both mechanisms ultimately leading to cell death via apoptosis or necrosis mechanisms.<sup>3</sup> For optimal clinical applications, the PS should undergo excitation at long wavelengths to minimize toxicity to healthy cells and afford deep tissue penetration,<sup>4</sup> and in addition to producing reactive oxygen species (ROS), it should be capable of fluorescing to permit image guidance alongside PDT, a feature often used to determine the optimal irradiation time and to assess the degree of cell death.<sup>5</sup>

Phenalenone (PN) (also known as 1*H*-phenalen-1-one or perinaphthenone) represents a class of natural products widely found in plants and fungi that possess antimicrobial roles as phytoalexins and phytoanticipins.<sup>6</sup> It is also well-known as an extremely efficient Type II photosensitizer having a near-unity singlet oxygen quantum yield across a wide range of solvents.<sup>7</sup> In fact, PNs have been described to display ROS-mediated activity against bacteria,<sup>8</sup> mosquito larvae,<sup>9</sup> parasitic nematodes,<sup>9,10</sup> and fungi<sup>11</sup> and more recently as a PDT agent against cancer.<sup>12,13</sup> In contrast to other types of PSs (e.g., porphyrins, BODIPYs, xanthenes),<sup>14</sup> the PN core structure is relatively

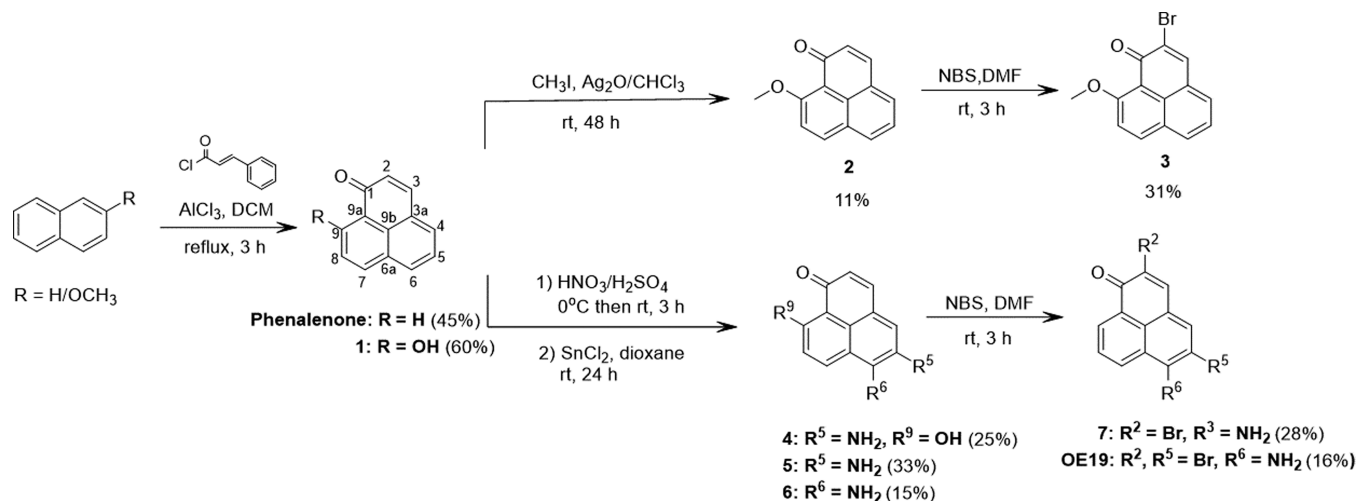
simple, comprising of three fused phenyl rings with one ketone, making it synthetically accessible, while its low molecular weight and relatively nonpolar nature make it capable of permeating cells for PDT.<sup>12</sup> However, the requirement of UV-A to violet light excitation (360–415 nm) limits PN for cancer treatment,<sup>15</sup> and its nonfluorescent nature does not permit real-time fluorescence imaging of cancerous tissue. Thus, a PN derivative capable of exerting high phototoxicity of cancer cells using long irradiation wavelengths (i.e., >415 nm) while permitting simultaneous fluorescence imaging is highly warranted.

Several groups have synthesized PN derivatives, which have provided some insight into the influence of substituents on the photophysical properties of PN. For example, it was found that the installation of methylene bridges does not lead to spectral red shifts or impact the PN singlet oxygen/fluorescence quantum yield.<sup>16–19</sup> In contrast, extending the  $\pi$  conjugation via ring substitution decreases the singlet oxygen yield<sup>13</sup> with no significant red shift in the absorption and only modest increases in fluorescence.<sup>13,20</sup> Sandoval-Altamirano et al. measured the photophysical behavior of hydroxy- and

Received: May 18, 2021

Accepted: July 7, 2021

## Scheme 1. Synthetic Pathway to Phenalenone Derivatives



ethoxy-PN derivatives in organic solvents<sup>21</sup> and found that these electron-donating groups cause red shifts and increase the fluorescence emission but reduce the singlet oxygen yield compared with native PN.<sup>21</sup> Unfortunately, whether these compounds have the ability to induce photocytotoxicity in cancer cells was not determined.

We sought to develop a PN derivative capable of absorbing long-wavelength light while producing sufficient singlet oxygen and fluorescence to kill and image cancer cells, respectively. Using the notion that electron-donating groups have the potential to cause spectral red shifts but undesirably reduce the singlet oxygen quantum yield, we reasoned the latter may be offset by the incorporation of heavy atoms to promote intersystem crossing to the triplet state<sup>22</sup> while not impacting the absorption spectrum significantly. To test this, we evaluated the effects of oxygen- and nitrogen-based electron donors in combination with bromination on the PN ring (Scheme 1). We note that although derivatives 1–3, 5, and 6 were previously synthesized, their singlet oxygen quantum yields were not determined.<sup>23–26</sup>

PN and derivative 1 were synthesized as previously reported by the reaction of commercially available *trans*-cinnamoyl chloride with either naphthalene or 2-methoxynaphthalene, respectively.<sup>25</sup> Methylation of derivative 1 with methyl iodide via an S<sub>N</sub>2 mechanism gave derivative 2,<sup>23</sup> and subsequent bromination using *N*-bromosuccinimide (NBS) yielded derivative 3.<sup>27</sup> To install an electron-donating amine group, compound 1 was nitrated through electrophilic aromatic substitution, which was directed to position 5 by the ortho/para electron-donating effect of the 9-hydroxy group. Subsequent reduction using SnCl<sub>2</sub> produced derivative 4.<sup>26</sup> A similar nitration and reduction procedure was performed on native PN, which yielded amino derivatives 5 and 6. Bromination of 5 and 6 using NBS yielded compound 7 and the key derivative OE19. NMR spectroscopy revealed that while derivative 5 was monobrominated at position 6, derivative 6 was dibrominated at positions 2 and 5 (see the Supporting Information). We note that monobromination of derivative 6 proved to be difficult, and thus, excess equivalents of NBS were introduced to push the reaction toward dibromination.

We determined the photophysical properties of each compound by first measuring their absorption spectra in

phosphate-buffered saline (PBS) containing 1% dimethyl sulfoxide (DMSO) (Tables 1 and 2). PN possesses an  $n \rightarrow$

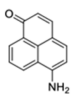
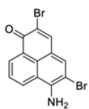
**Table 1. Absorption Maxima and Singlet Oxygen Quantum Yields of Phenalenone Derivatives 1–5 and 7<sup>a</sup>**

Derivative	Structure	$\lambda_{\max}$ (nm) in PBS	$\Phi_{\Delta} \pm$ S.D.
1		439	0.96 $\pm$ 0.06
2		418	0.68 $\pm$ 0.02
3		427	0.89 $\pm$ 0.06
4		485	< 0.01
5		457	0.18 $\pm$ 0.05
7		458	0.10 $\pm$ 0.05

<sup>a</sup>All of the experiments were performed at room temperature in PBS (pH 7.4). The reference for derivatives 1–5 and 7 was phenalenone ( $\Phi_{\Delta} \approx 1$ ).<sup>7</sup> The reference for derivative 4 was eosin Y ( $\Phi_{\Delta} \approx 0.57$ ).<sup>29</sup>

$\pi^*$  transition from 330 to 430 nm ( $\lambda_{\max} = 360$  nm) with an extinction coefficient of 10 000 M<sup>-1</sup> cm<sup>-1</sup>.<sup>17,28</sup> We found that all of the derivatives having the addition of electron-donating groups (hydroxy, methoxy, amino), regardless of position on the ring, exhibited a red shift of the  $n \rightarrow \pi^*$  band compared with native PN (Figures 1 and S1–S3). As expected, bromination did not significantly impact the absorption spectra compared with the corresponding parent scaffolds (2 vs 3, 5 vs 7, and 6 vs OE19). Installation of the amine at the 5-position (i.e., 5) produced a red shift of  $\sim$ 100 nm relative to PN, which increased to 125 nm when there was a hydroxyl group at the 9-position (i.e., 4). Interestingly, moving the amine from the 5-position to the 6-position (i.e., 6) induced an additional  $\sim$ 100 nm red shift in the absorption spectrum, thereby producing the most red-shifted compound in our series.

Table 2. Photophysical Properties of Compound 6 and OE19<sup>a</sup>

	Compound 6	OE19
		
$\lambda_{\text{max}}$ (nm) in PBS	548	546
$\lambda_{\text{max}}$ (nm) in DMSO	518	525
$\Phi_{\Delta} \pm \text{S.D.}^b$	< 0.01	$0.47 \pm 0.04$
$\Phi_f \pm \text{S.D.}^b$	$0.26 \pm 0.02$	$0.29 \pm 0.02$
$\lambda_{\text{em. max.}}$ (nm) <sup>b</sup>	597	602
$\epsilon$ (M <sup>-1</sup> cm <sup>-1</sup> )	12736 <sup>c</sup>	12695 <sup>d</sup>

<sup>a</sup>All of the experiments were performed at room temperature. <sup>b</sup> $\Phi_{\Delta}$ ,  $\Phi_f$  and  $\lambda_{\text{em. max.}}$  were measured in DMSO. The reference for the <sup>1</sup>O<sub>2</sub> quantum yield was rose bengal ( $\Phi_{\Delta} = 0.76$ ), and rhodamine B ( $\Phi_f = 0.5$ ) was the reference for the fluorescence quantum yield.<sup>32</sup> <sup>c</sup>Determined in PBS.<sup>26</sup> <sup>d</sup>Determined in PBS with 100  $\mu\text{g/mL}$  BSA.

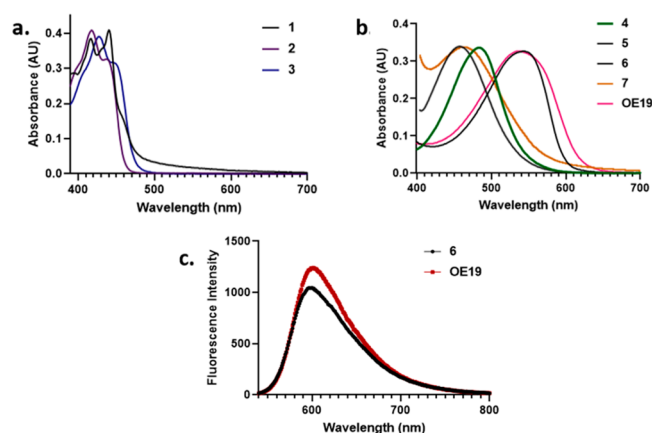


**Figure 1.** Spectra of phenalenone derivatives. (a) Lowest-energy absorption band of hydroxy- or methoxy-PN compounds 1–3 in PBS. (b) Lowest-energy absorption band of amino-containing compounds 4–7 and OE19 in PBS. (c) Fluorescence spectra of compound 6 and OE19 in DMSO after excitation at 518 and 525 nm (0.13 AU at each maximum), respectively.

We next determined the singlet oxygen quantum yields of our derivatives using the singlet oxygen sensor 9,10-anthracenediylbis(methylene)dimalonic acid (ABDA). ABDA is selectively photobleached by singlet oxygen into its corresponding endoperoxide, turning off its characteristic absorption.<sup>30</sup> Thus, a decrease the ABDA absorption at 401 nm can be monitored with increasing irradiation time for each derivative, and the resulting slopes can be compared with those of standards with known quantum yields irradiated under the same conditions (Figures S4–S6). Although the introduction of the electron-donating 9-hydroxy group in 1 produced a bathochromic shift, it did not largely affect the singlet oxygen production efficiency compared with native PN (Table 1). In contrast, methylation of the hydroxy group to generate the

methoxy group (2) did cause a decrease in the singlet oxygen yield. However, the singlet oxygen yield was nearly recovered by the addition of Br at the 2-position (3), in agreement with our initial hypothesis.

Addition of the more strongly electron-donating amino group at the 5-position (5) led to a decrease in the singlet oxygen yield, and adding the 9-hydroxy group (4) abolished the singlet-oxygen-generating capability. Unfortunately, unlike compound 2 versus 3, the introduction of bromine at the 6-position (i.e., 7) could not recover the singlet oxygen production but rather led to a decrease in the yield compared with 5. This result suggests that the ability of a bromine substituent to induce intersystem crossing and subsequent singlet oxygen production depends on the position of the bromine on the PN scaffold. Such a position dependence has been previously observed for BODIPY-based PSs.<sup>31</sup>

Similar to derivative 4, direct modification of the  $\pi$  ring system with the electron-donating amino group at the 6-position (6) led to a complete loss of singlet oxygen production. However, in this case, bromination at the 2- and 5-positions (OE19) resulted in a significant increase in the singlet oxygen yield. Since previously characterized 6 is known to be a good fluorophore,<sup>26</sup> we asked whether the increase in singlet oxygen production in OE19 came at the expense of fluorescence. Interestingly, OE19 was found to retain fluorescence emission at  $\sim 600$  nm with a quantum yield similar to that of its parent compound 6, while compounds 1–5 and 7 did not exhibit any significant fluorescence ( $\Phi_f < 0.05$ ). Thus, among the derivatives synthesized, OE19 exhibits the best combination of long-wavelength absorption and good fluorescence and singlet oxygen quantum yields, making it the most promising candidate in the series.

The above photophysical properties of OE19 were measured in DMSO, as solubility/aggregation was found to occur in PBS (although 6 was stable in PBS, measurements were performed in DMSO for better comparison to OE19). Specifically, we observed the fluorescence of OE19 to decrease with time in PBS (Figure S7), which also resulted in a reduction in singlet oxygen production (Figure S8). However, we found that this aggregation effect can be diminished by the addition of bovine serum albumin (BSA) to the PBS or by dissolving OE19 in cell medium (DMEM) containing 10% fetal bovine serum (FBS) (Figure S9). These results are consistent with studies using high-protein environments as preventative measures against small-molecule aggregation,<sup>33,34</sup> as dissolving OE19 in medium with reduced serum (Opti-MEM) or no serum at all resulted in aggregation (Figure S9). Thus, given these observations, we reasoned that OE19 may still function in cells, where intracellular molecular crowding would reduce aggregation, thereby permitting fluorescence and singlet oxygen production. We note that under our irradiation conditions, the absorbance of OE19 in PBS containing BSA remained constant, suggesting that OE19 exhibits high photostability (Figure S10), a characteristic that is also desirable for cellular applications.

To test OE19 in cells, we prepared a stock solution in DMSO, which was diluted to a final concentration of 2  $\mu\text{M}$  in wells containing the pancreatic cancer cell line PANC-1 in reduced-serum medium (Opti-MEM). After incubation for 3 h, we observed bright red fluorescence signals diffuse within the cytosol, suggesting that OE19 is cell-permeable (Figure 2). Interestingly, we also observed good fluorescence contrast of cells without removal of OE19 from the medium. We hypothesize that this is likely the case because although

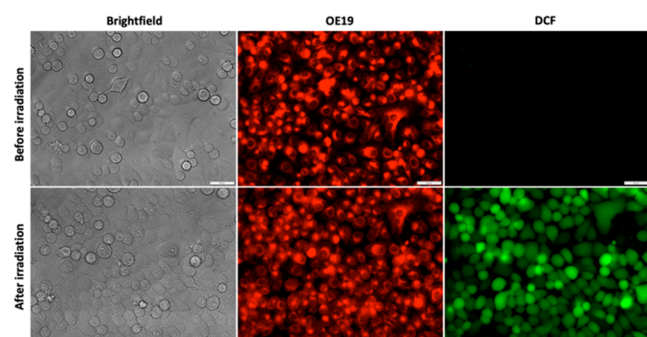


**Figure 2.** Fluorescence imaging of **OE19** and intracellular ROS production in PANC-1 cells. Top row: before irradiation, bright red fluorescence from **OE19** ( $2 \mu\text{M}$ ) was observed, but no green fluorescence from DCF (the product of ROS oxidation and esterase cleavage from  $\text{DCFH}_2\text{-DA}$ ) was observed. Bottom row: after irradiation ( $530 \text{ nm}$ ,  $10 \text{ min}$ ,  $11.14 \text{ J/cm}^2$ ), bright green fluorescence from DCF was observed, indicative of ROS production by **OE19**. Scale bar =  $50 \mu\text{m}$ .

aggregation of **OE19** occurs in reduced-serum medium, leading to fluorescence quenching (Figure S9), the intracellular environment is capable of reducing the aggregation, thereby “turning on” the fluorescence. Given these promising results, we next determined whether **OE19** is capable of producing ROS intracellularly by employing the cell-permeable ROS sensor 2',7'-dichlorofluorescein diacetate ( $\text{DCFH}_2\text{-DA}$ ). When  $\text{DCFH}_2\text{-DA}$  is deacetylated by intracellular esterases and oxidized by ROS, the green-fluorescent product 2',7'-dichlorofluorescein (DCF) is produced.<sup>35</sup> Irradiation of PANC-1 cells treated with both  $\text{DCFH}_2\text{-DA}$  and **OE19** produced substantially stronger green fluorescence in comparison with PANC-1 cells treated without irradiation (Figure 2) or treated with only  $\text{DCFH}_2\text{-DA}$  or **OE19** and irradiated (Figures S11 and S12). To evaluate whether the light-induced ROS production by **OE19** can induce photocytotoxicity, PANC-1 cells were treated with **OE19** ( $0\text{--}2 \mu\text{M}$ ) in the dark or with green-light irradiation (using a lamp with a green filter with an emission maximum at  $525 \text{ nm}$ ,  $16.61 \text{ J/cm}^2$ ) for  $15 \text{ min}$ . After the cells were cultured in the dark for  $24 \text{ h}$ , the cell viability was determined using a standard MTT assay. We found that irradiation induced cytotoxicity in a dose-dependent manner with nanomolar potency ( $\text{IC}_{50} = 166 \text{ nM}$ ) (Figure 3). In contrast, cells treated and kept in the dark displayed no significant dark toxicity ( $\text{IC}_{50} > 2 \mu\text{M}$ ) (Figure 3).

The mechanism of cell death was investigated by employing annexin V-FITC, which binds to phosphatidylserine translocated to cell membrane exteriors during apoptosis, producing green fluorescence.<sup>36</sup> Cells were also stained with propidium iodide, which permeates only damaged cell and nuclear membranes.<sup>37</sup> However, since propidium iodide and **OE19** have overlapping emission, red fluorescence in the nuclei was used only to confirm cell death (Figure S13). PANC-1 cells were incubated with  $0.5 \mu\text{M}$  **OE19**, irradiated for  $15 \text{ min}$  with green light (using a lamp with a green filter with an emission maximum at  $525 \text{ nm}$ ,  $16.61 \text{ J/cm}^2$ ), and then stained with annexin V-FITC  $30 \text{ min}$ ,  $80 \text{ min}$ ,  $3 \text{ h}$ , or  $24 \text{ h}$  after PDT. We observed green fluorescence over background at all time points, with the strongest signals produced at  $24 \text{ h}$ , suggesting that the cells died by apoptosis (Figure 4). PANC-1 cells incubated with **OE19** ( $0.5 \mu\text{M}$ ,  $3 \text{ h}$ ) but kept in the dark lacked

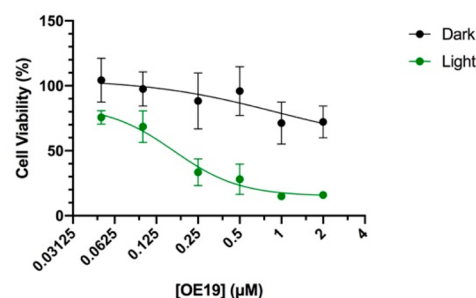


**Figure 3.** Cell viability of PANC-1 cancer cells. Cells were treated with increasing concentrations ( $0\text{--}2 \mu\text{M}$ ) of **OE19** in the dark or under light conditions ( $15 \text{ min}$  using a lamp with a green filter with an emission maximum at  $525 \text{ nm}$ ,  $16.61 \text{ J/cm}^2$ ). Cells treated with **OE19** displayed a dose-dependent response in viability under light ( $\text{IC}_{50} = 166 \text{ nM}$ ) but not in the dark ( $\text{IC}_{50} > 2 \mu\text{M}$ ). Data are presented as mean  $\pm$  SD ( $n = 9$ ).

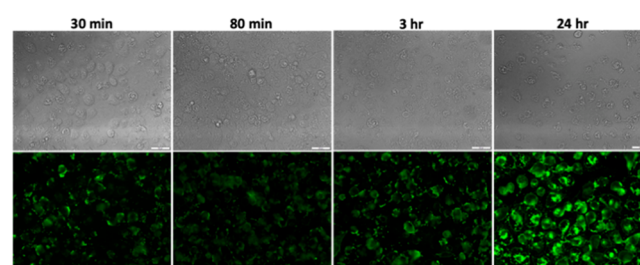


**Figure 4.** Mechanism of cell death. PANC-1 cells were stained with annexin V-FITC after treatment with **OE19** ( $0.5 \mu\text{M}$ ) and irradiation for  $15 \text{ min}$  with green light (using a lamp with a green filter with an emission maximum at  $525 \text{ nm}$ ,  $16.61 \text{ J/cm}^2$ ). Shown are (top row) bright-field images and (bottom row) fluorescence images of cells stained with annexin V-FITC  $30 \text{ min}$ ,  $80 \text{ min}$ ,  $3 \text{ h}$ , and  $24 \text{ h}$  after irradiation.  $20\times$  magnification, scale bars =  $50 \mu\text{m}$ .

green emission from annexin-V-FITC, indicating that no dark toxicity was exerted by **OE19** (Figure S14).

Encouraged by the high potency and large light–dark therapeutic window of **OE19**, we further explored its ability to exert photocytotoxicity on PANC-1 tumor spheroids. Compared with 2D cell culture, 3D cell culture systems more accurately represent the microenvironment of tumors with respect to their cell physiology, morphology, and spatial dimensionality, and therefore, spheroids are regarded as a better assessment of the in vivo therapeutic potential of compounds.<sup>38</sup> PANC-1 spheroids treated with **OE19** ( $0\text{--}1.5 \mu\text{M}$ ) for  $3 \text{ h}$  and kept in the dark exhibited no observable changes in diameter or overall changes in cell density as determined by bright-field images (Figure 5a,c). To further confirm the cell viability of the spheroid, we used the commercially available ReadyProbes Cell Viability Imaging Kit, Blue/Green, whereby Hoechst 33342 fluorescently stains the nuclei of viable and dead cells blue, while only dead cells are stained with a green fluorescent nuclear dye. Cell death staining of these spheroids showed bright blue fluorescent signals with no observable green fluorescent signals, confirming viability of the spheroids (Figure 5a,c). In contrast, spheroids treated with **OE19** ( $0\text{--}1.5 \mu\text{M}$ ,  $3 \text{ h}$  incubation) and exposed to green-light irradiation (using a lamp with a green filter with an emission maximum at  $525 \text{ nm}$ ,  $16.61 \text{ J/cm}^2$ ) for  $15 \text{ min}$  showed a decreasing trend in diameter and a difference in morphology of the spheroids, with total spheroid breakage

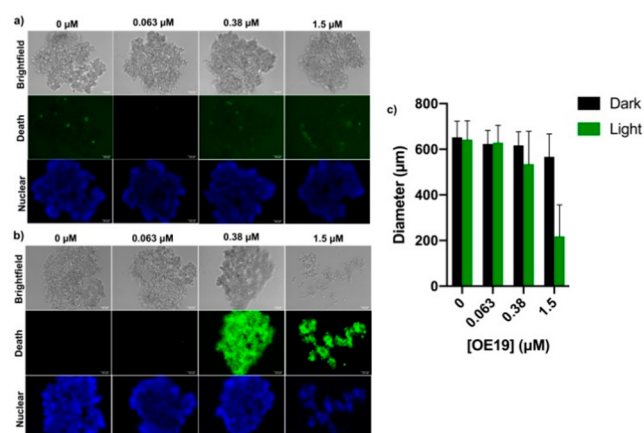


**Figure 5.** PDT in PANC-1 tumor spheroids. (a) Spheroids treated with OE19 (0–1.5  $\mu\text{M}$ ) under dark conditions: (top row) bright-field images with no observable breakage; (middle row) no cell death was observed using the green fluorescent cell death reagent from the ReadyProbes Cell Viability Imaging Kit Blue/Green; (bottom panel) nuclear staining of all cells by Hoechst 33342. (b) Spheroids treated with OE19 (0–1.5  $\mu\text{M}$ ) after irradiation (using a lamp with a green filter with an emission maximum at 525 nm, 16.61 J/cm<sup>2</sup>) for 15 min: (top row) bright-field images show changes in spheroid morphology and density in a dose-dependent manner; (middle row) green emission indicative of cell death was observed at 0.38 and 1.5  $\mu\text{M}$ ; (bottom row) blue emission from the nuclei of all cells by Hoechst 33342 using the ReadyProbes Cell Viability Imaging Kit. 10 $\times$  magnification, scale bars = 100  $\mu\text{m}$ . (c) Quantification of spheroid diameter after treatment with OE19 in the dark or after irradiation. Bars represent averages of three replicate spheroids for each condition with 12 diameter measurements of each spheroid, and error bars represent their respective standard deviations. No significant change in diameter was observed in the dark.

observed upon treatment with 1.5  $\mu\text{M}$  OE19 and light (Figure 5b,c). Live/dead cell staining revealed a high degree of photocytotoxicity for spheroids treated with 0.38 and 1.5  $\mu\text{M}$  OE19, consistent with the observed morphological changes (Figure 5b).

In summary, we have developed the first long wavelength (i.e., green)-absorbing red-fluorescent PN derivative capable of producing singlet oxygen upon light irradiation. OE19 is cell-permeable and exerts a high degree of photocytotoxicity in both 2D and 3D cultured PANC-1 cancer cells with minimal dark toxicity. OE19 was discovered by an examination of the effects of electron-donating groups with or without bromination at various positions on the PN scaffold. Much like native PN, its synthesis is simple, requiring only four steps using commercially available, inexpensive reagents. For PDT applications in vivo, we acknowledge that OE19 falls short with regard to light excitation within the biological optical window and suffers from limited solubility for administration. However, since the derivatives synthesized here also provide insight into the relationship between the intrinsic molecular electronic structure of PN and its photophysical properties, it seems possible that further exploration may lead to a PN derivative capable of produce singlet oxygen with red- or NIR-light irradiation. Further derivatization can also be done to improve the solubility of OE19, such as installation of a methylene bridge containing moieties bearing charges at pH 7.4 (e.g., a sulfonate or amino group). Lastly, aside from the enhanced permeability and retention effect, OE19 is not expected to exhibit a high degree of cancer selectivity over

healthy cells. However, it may be possible to modify the 6-amino functional group with substrates for overexpressed enzymes found in cancer cells, such as quinones for NQO1<sup>16</sup> or amino acids for peptidases,<sup>39</sup> as a means to achieve selectivity.

## ■ ASSOCIATED CONTENT

### Supporting Information

The Supporting Information is available free of charge at <https://pubs.acs.org/doi/10.1021/acsmchemlett.1c00284>.

Synthetic details; <sup>1</sup>H NMR, <sup>13</sup>C NMR, and HRMS spectra; photophysical characterization experiments; absorption spectra; singlet oxygen and fluorescence quantum yield measurements; solubility assessments; cell culture details and imaging experiments; cell viability in 2D and 3D PANC-1 cell culture experiments (PDF)

## ■ AUTHOR INFORMATION

### Corresponding Author

Andrew A. Beharry – Department of Chemical and Physical Sciences, University of Toronto Mississauga, Mississauga, ON L5L 1C6, Canada; Department of Chemistry, University of Toronto, Toronto, ON M5S 3H6, Canada;  
Email: [andrew.beharry@utoronto.ca](mailto:andrew.beharry@utoronto.ca)

### Authors

Esther G. Kaye – Department of Chemical and Physical Sciences, University of Toronto Mississauga, Mississauga, ON L5L 1C6, Canada; Department of Chemistry, University of Toronto, Toronto, ON M5S 3H6, Canada  
Karishma Kailass – Department of Chemical and Physical Sciences, University of Toronto Mississauga, Mississauga, ON L5L 1C6, Canada; Department of Chemistry, University of Toronto, Toronto, ON M5S 3H6, Canada  
Oleg Sadovski – Department of Chemical and Physical Sciences, University of Toronto Mississauga, Mississauga, ON L5L 1C6, Canada; Department of Chemistry, University of Toronto, Toronto, ON M5S 3H6, Canada

Complete contact information is available at: <https://pubs.acs.org/doi/10.1021/acsmchemlett.1c00284>

### Author Contributions

The experiments were designed by E.G.K., K.K., and A.A.B. Synthesis was completed by O.S. and E.G.K. Photophysical measurements and cell culture experiments were completed by E.G.K. and K.K. The manuscript was written by E.G.K., K.K., and A.A.B. All of the authors approved the final version of the manuscript.

### Notes

The authors declare no competing financial interest.

## ■ ACKNOWLEDGMENTS

Funding through a Natural Sciences and Engineering Research Council of Canada (NSERC) Discovery Grant is acknowledged. K.K. acknowledges support from NSERC Postgraduate Scholarship - Doctoral (PGS-D). E.G.K. acknowledges support from the University of Toronto Excellence Award (UTEA).

## ■ ABBREVIATIONS

PDT, photodynamic therapy; PS, photosensitizer; ROS, reactive oxygen species; UV-A, ultraviolet A; NMR, nuclear magnetic resonance; LED, light-emitting diode; ABDA, 9,10-

anthracenediylbis(methylene)dimalonic acid; DMSO, dimethyl sulfoxide; DCF, 2',7'-dichlorofluorescein; DCFH<sub>2</sub>-DA, 2',7'-dichlorodihydrofluorescein diacetate; MTT, 3-(4,5-dimethylthiazol-2-yl)-2,5-diphenyltetrazolium bromide; IC<sub>50</sub>, half-maximal inhibitory concentration; FITC, fluorescein isothiocyanate

## REFERENCES

- (1) Dougherty, T. J.; Marcus, S. L. Photodynamic Therapy. *Eur. J. Cancer* **1992**, *28* (10), 1734–1742.
- (2) Zhao, J.; Wu, W.; Sun, J.; Guo, S. Triplet Photosensitizers: From Molecular Design to Applications. *Chem. Soc. Rev.* **2013**, *42* (12), 5323–5351.
- (3) Soriano, J.; Mora-Espí, I.; Alea-Reyes, M. E.; Pérez-García, L.; Barrios, L.; Ibáñez, E.; Nogués, C. Cell Death Mechanisms in Tumoral and Non-Tumoral Human Cell Lines Triggered by Photodynamic Treatments: Apoptosis, Necrosis and Parthanatos. *Sci. Rep.* **2017**, *7*, 41340.
- (4) Kobayashi, H.; Ogawa, M.; Alford, R.; Choyke, P. L.; Urano, Y. New Strategies for Luminescence Probe for In Vivo Imaging. *Chem. Rev.* **2010**, *110* (5), 2620–2640.
- (5) Lovell, J. F.; Liu, T. W. B.; Chen, J.; Zheng, G. Activatable Photosensitizers for Imaging and Therapy. *Chem. Rev.* **2010**, *110* (5), 2839–2857.
- (6) Flors, C.; Nonell, S. Light and Singlet Oxygen in Plant Defense against Pathogens: Phototoxic Phenalenone Phytoalexins. *Acc. Chem. Res.* **2006**, *39* (5), 293–300.
- (7) Schmidt, R.; Tanielian, C.; Dunsbach, R.; Wolff, C. Phenalenone, a Universal Reference Compound for the Determination of Quantum Yields of Singlet Oxygen O<sub>2</sub>(<sup>1</sup>Δ<sub>g</sub>) Sensitization. *J. Photochem. Photobiol., A* **1994**, *79*, 11–17.
- (8) Quiñones, W.; Escobar, G.; Echeverri, F.; Torres, F.; Rosero, Y.; Arango, V.; Cardona, G.; Gallego, A. Synthesis and Antifungal Activity of Musa Phytoalexins and Structural Analogs. *Molecules* **2000**, *5* (7), 974–980.
- (9) Song, R.; Feng, Y.; Wang, D.; Xu, Z.; Li, Z.; Shao, X. Phytoalexin Phenalenone Derivatives Inactivate Mosquito Larvae and Root-Knot Nematode as Type-II Photosensitizer. *Sci. Rep.* **2017**, *7*, 42058.
- (10) Hölscher, D.; Dhakshinamoorthy, S.; Alexandrov, T.; Becker, M.; Bretschneider, T.; Buerkert, A.; Crecelius, A. C.; De Waele, D.; Elsen, A.; Heckel, D. G.; Heklau, H.; Hertweck, C.; Kai, M.; Knop, K.; Krafft, C.; Maddula, R. K.; Matthäus, C.; Popp, J.; Schneider, B.; Schubert, U. S.; Sikora, R. A.; Svatoš, A.; Swennen, R. L. Phenalenone-Type Phytoalexins Mediate Resistance of Banana Plants (*Musa Spp.*) to the Burrowing Nematode *Radopholus Similis*. *Proc. Natl. Acad. Sci. U. S. A.* **2014**, *111* (1), 105–110.
- (11) Lazzaro, A.; Corominas, M.; Martí, C.; Flors, C.; Izquierdo, L. R.; Grillo, T. A.; Luis, J. G.; Nonell, S. Light- and Singlet Oxygen-Mediated Antifungal Activity of Phenylphenalenone Phytoalexins. *Photochem. Photobiol. Sci.* **2004**, *3* (7), 706–710.
- (12) Salmerón, M. L.; Quintana-Aguir, J.; De La Rosa, J. V.; López-Blanco, F.; Castrillo, A.; Gallardo, G.; Tabraue, C. Phenalenone-Photodynamic Therapy Induces Apoptosis on Human Tumor Cells Mediated by Caspase-8 and P38-MAPK Activation. *Mol. Carcinog.* **2018**, *57* (11), 1525–1539.
- (13) Jing, Y.; Xu, Q.; Chen, M.; Shao, X. Pyridone-Containing Phenalenone-Based Photosensitizer Working Both under Light and in the Dark for Photodynamic Therapy. *Bioorg. Med. Chem.* **2019**, *27* (11), 2201–2208.
- (14) Zhang, J.; Jiang, C.; Figueiró Longo, J. P.; Azevedo, R. B.; Zhang, H.; Muehlmann, L. A. An Updated Overview on the Development of New Photosensitizers for Anticancer Photodynamic Therapy. *Acta Pharm. Sin. B* **2018**, *8* (2), 137–146.
- (15) Moan, J.; Peak, M. J. Effects of UV Radiation on Cells. *J. Photochem. Photobiol., B* **1989**, *4* (1), 21–34.
- (16) Digby, E. M.; Sadovski, O.; Beharry, A. A. An Activatable Photosensitizer Targeting Human NAD(P)H: Quinone Oxidoreductase 1. *Chem. - Eur. J.* **2020**, *26* (12), 2713–2718.
- (17) Godard, J.; Brégier, F.; Arnoux, P.; Myrzakhmetov, B.; Champavier, Y.; Frochet, C.; Sol, V. New Phenalenone Derivatives: Synthesis and Evaluation of Their Singlet Oxygen Quantum Yield. *ACS Omega* **2020**, *5* (43), 28264–28272.
- (18) Godard, J.; Chapron, D.; Bregier, F.; Rosilio, V.; Sol, V. Synthesis and Supramolecular Arrangement of New Stearoyl Acid-Based Phenalenone Derivatives. *Colloids Surf., A* **2021**, *612*, 125988.
- (19) Godard, J.; Gibbons, D.; Leroy-Lhez, S.; Williams, R. M.; Villandier, N.; Ouk, T.-S.; Brégier, F.; Sol, V. Development of Phenalenone-Triazolium Salt Derivatives for aPDT: Synthesis and Antibacterial Screening. *Antibiotics* **2021**, *10*, 626.
- (20) Phatangare, K. R.; Lanke, S. K.; Sekar, N. Phenalenone Fluorophores-Synthesis, Photophysical Properties and DFT Study. *J. Fluoresc.* **2014**, *24* (6), 1827–1840.
- (21) Sandoval-Altamirano, C.; De la Fuente, J. R.; Berrios, E.; Sanchez, S. A.; Pizarro, N.; Morales, J.; Gunther, G. Photophysical Characterization of Hydroxy and Ethoxy Phenalenone Derivatives. *J. Photochem. Photobiol., A* **2018**, *353*, 349–357.
- (22) Koziar, J. C.; Cowan, D. Photochemical Heavy-Atom Effects. *Acc. Chem. Res.* **1978**, *11* (9), 334–341.
- (23) Franz, K. D.; Martin, R. L. 1,9-Disubstituted Phenalenes—I: Synthesis of N- and S-Derivatives of 9-Hydroxy-1-phenalenone. *Tetrahedron* **1978**, *34* (14), 2147–2151.
- (24) Lebraud, H.; Wright, D. J.; Johnson, C. N.; Heightman, T. D. Protein Degradation by In-Cell Self-Assembly of Proteolysis Targeting Chimeras. *ACS Cent. Sci.* **2016**, *2* (12), 927–934.
- (25) Haddon, R. C.; Rayford, R.; Hirani, A. M. 2-Methyl- and 5-Methyl-9-hydroxyphenalenone. *J. Org. Chem.* **1981**, *46* (22), 4587–4588.
- (26) Kailass, K.; Sadovski, O.; Capello, M.; Kang, Y.; Fleming, J. B.; Hanash, S. M.; Beharry, A. A. Measuring Human Carboxylesterase 2 Activity in Pancreatic Cancer Patient-Derived Xenografts Using a Ratiometric Fluorescent Chemosensor. *Chem. Sci.* **2019**, *10* (36), 8428–8437.
- (27) Ospina, F.; Hidalgo, W.; Cano, M.; Schneider, B.; Otlávaro, F. Synthesis of 8-Phenylphenalenes: 2-Hydroxy-8-(4-hydroxyphenyl)-1H-phenalen-1-one from *Eichhornia crassipes*. *J. Org. Chem.* **2016**, *81* (3), 1256–1262.
- (28) Daza, M. C.; Doerr, M.; Salzmann, S.; Marian, C. M.; Thiel, W. Photophysics of Phenalenone: Quantum-Mechanical Investigation of Singlet-Triplet Intersystem Crossing. *Phys. Chem. Chem. Phys.* **2009**, *11* (11), 1688–1696.
- (29) Wilkinson, F.; Helman, W. P.; Ross, A. B. Quantum Yields for the Photosensitized Formation of the Lowest Electronically Excited Singlet State of Molecular Oxygen in Solution. *J. Phys. Chem. Ref. Data* **1993**, *22* (1), 113–262.
- (30) Entradas, T.; Waldron, S.; Volk, M. The Detection Sensitivity of Commonly Used Singlet Oxygen Probes in Aqueous Environments. *J. Photochem. Photobiol., B* **2020**, *204*, No. 111787.
- (31) Prieto-Montero, R.; Prieto-Castañeda, A.; Sola-Llano, R.; Agarrabaitia, A. R.; García-Fresnadillo, D.; López-Arbeloa, I.; Villanueva, A.; Ortiz, M. J.; de la Moya, S.; Martínez-Martínez, V. Exploring BODIPY Derivatives as Singlet Oxygen Photosensitizers for PDT. *Photochem. Photobiol.* **2020**, *96* (3), 458–477.
- (32) Brouwer, A. M. Standards for Photoluminescence Quantum Yield Measurements in Solution (IUPAC Technical Report). *Pure Appl. Chem.* **2011**, *83* (12), 2213–2228.
- (33) McGovern, S. L.; Caselli, E.; Grigorieff, N.; Shoichet, B. K. A Common Mechanism Underlying Promiscuous Inhibitors from Virtual and High-Throughput Screening. *J. Med. Chem.* **2002**, *45* (8), 1712–1722.
- (34) Coan, K. E. D.; Shoichet, B. K. Stability and Equilibria of Promiscuous Aggregates in High Protein Milieus. *Mol. Biosyst.* **2007**, *3* (3), 208–213.
- (35) LeBel, C. P.; Ischiropoulos, H.; Bondy, S. C. Evaluation of the Probe 2',7'-Dichlorofluorescein as an Indicator of Reactive Oxygen Species Formation and Oxidative Stress. *Chem. Res. Toxicol.* **1992**, *5* (2), 227–231.

(36) Koopman, G.; Reutelingsperger, C. P. M.; Kuijten, G. A. M.; Keehnen, R. M. J.; Pals, S. T.; Van Oers, M. H. J. Annexin V for Flow Cytometric Detection of Phosphatidylserine Expression on B Cells Undergoing Apoptosis. *Blood* **1994**, *84* (5), 1415–1420.

(37) Nicoletti, I.; Migliorati, G.; Pagliacci, M. C.; Grignani, F.; Riccardi, C. A Rapid and Simple Method for Measuring Thymocyte Apoptosis by Propidium Iodide Staining and Flow Cytometry. *J. Immunol. Methods* **1991**, *139* (2), 271–279.

(38) Edmondson, R.; Broglie, J. J.; Adcock, A. F.; Yang, L. Three-Dimensional Cell Culture Systems and Their Applications in Drug Discovery and Cell-Based Biosensors. *Assay Drug Dev. Technol.* **2014**, *12* (4), 207–218.

(39) Fujita, K.; Kamiya, M.; Urano, Y. Rapid and Sensitive Detection of Cancer Cells with Activatable Fluorescent Probes for Enzyme Activity. *Methods Mol. Biol.* **2021**, *2274*, 193–206.